Journal of Engineering and Applied Science

RESEARCH Open Access

Experimental and CFD analysis of cavitation in three-lobe journal bearings lubricated with and without TiO_2 nanolubricants

N. B. Ahire[1] and D. D. Deshmukh[1*]

*Correspondence:
D. D. Deshmukh
dhirgajanan@gmail.com
[1]MET's Institute of Engineering, Nashik, SPPU, Pune, MS 422003, India

Abstract

Hydrodynamic journal bearings (HJBs) are widely used in high-speed rotating machinery owing to their high load capacity and vibration suppression capabilities; however, cavitation in the diverging film region often undermines their performance and reliability. This study presents an integrated experimental numerical investigation of three-lobe HJBs lubricated with titanium dioxide (TiO_2)-based nanofluids and Mobil DTE 24 oil at 500, 750 and 1000 RPM. Circumferential pressure distributions were measured using an experimental test rig for base oil (Mobil DTE 24) and a 0.5 wt.% TiO_2 nanolubricant. Also, CFD simulations were carried out in ANSYS employing a mixture multiphase model coupled with the Zwart Gerber Belamri (ZGB) cavitation model. The results showed that TiO_2 nanoparticles increased peak hydrodynamic pressures, alleviated negative pressures in diverging zones and significantly suppressed cavitation across all operating speeds. Numerical predictions closely matched experimental measurements, with deviations within ± 6%, validating the adopted computational methodology. Pressure profiles further indicated enhanced film stability and improved load-carrying capacity with nanoparticle addition. This study provides benchmark data on the performance of nanolubricants in three-lobe HJBs. It also shows that combining experiments with CFD is an effective approach for evaluating advanced lubrication strategies. The findings provide practical guidance for improving bearing design and increasing reliability in moderate-speed industrial applications.

Keywords Three-lobe journal bearing, TiO_2 nanolubricants, CFD, Cavitation effect, Hydrodynamic lubrication

Introduction

Hydrodynamic journal bearings (HJBs) are vital components in rotating machinery, where a thin lubricant film separates the shaft from the bearing surface to sustain heavy loads and minimize direct contact [1, 2]. They are extensively employed in turbines, compressors, marine propulsion systems, and pumps, where their ability to carry high radial loads and suppress vibrations ensure reliable operation [1, 3]. However, conventional cylindrical bearings often exhibit instabilities such as oil whirl, cavitation, and

excessive power loss at elevated speeds. To mitigate these drawbacks, multi-lobe designs have been developed. In particular, three-lobe bearings introduce inherent preload and segmented pressure zones, which have been reported to improve film stiffness and enhance stability margins [3–6]. Despite these advantages, most investigations on TiO_2-based nanolubricants have been carried out on plain and elliptical bearings [7–9], while the cavitation-prone three-lobe configuration remains underexplored. Experimental studies have confirmed that TiO_2 nanoparticles can increase load capacity and reduce friction [7, 10], but cavitation dynamics were not incorporated into these analyses. High-speed CFD investigations of TiO_2/ZnO nanofluids [9] have obtained encouraging results; however, systematic evaluations at moderate speeds ($N < 1000$ RPM), which are highly relevant to industrial practice, are still rare. Furthermore, direct comparisons of base oils and nanolubricants under identical test conditions remain limited [11, 12], restricting the ability to isolate nanoparticle-specific effects.

Experimental validation has consistently been observed as a critical step for assessing CFD predictions of journal bearing behavior. For instance, Shaltout and Hegazi [13] demonstrated that combined experimental and numerical approaches can provide reliable performance assessments, while Dhande et al. [5] carried out fluid structure interaction (FSI) analyses that achieved close agreement with recorded pressure profiles. Related investigations further highlight the importance of cavitation modeling in predicting elastohydrodynamic and multiphase flow behavior [14, 15]. The ZGB cavitation model has since been established as a widely accepted framework for simulating vapor inception and collapse in hydrodynamic bearings [16–18]. In parallel, the use of nanolubricants has been confirmed to enhance viscosity stability, thermal conductivity, and load capacity [19–21]. TiO_2 nanoparticles, in particular, have demonstrated favorable tribological and thermal characteristics, and several studies have reported their ability to suppress cavitation and reduce frictional losses at low concentrations [22–26]. Complementary reviews and numerical investigations have emphasized the role of non-circular bearing geometries [27] and advanced viscosity models [28] in improving stability margins, offering further insights into lubricant–geometry interactions.

In this context, the present study was carried out to investigate the performance of three-lobe journal bearings lubricated with TiO_2 nanofluids at moderate speeds. Hydrodynamic pressures were recorded using a test setup and compared against numerical predictions obtained through CFD simulations in ANSYS Fluent employing the ZGB cavitation model. Also, this study advances the current understanding of hydrodynamic lubrication in multi-lobe bearings by integrating experimental and CFD investigations using TiO_2-based nanolubricants. Unlike previous studies that primarily focused on plain or elliptical bearings [9, 11, 17]. The focus is given in the present work to investigate detailed three-lobe bearing pressure distribution under varying speeds and lubrication conditions. The validated CFD–ZGB cavitation framework exhibits close agreement with experimental measurements and reveals the mechanisms by which TiO_2 nanoparticles enhance pressure build-up and suppress cavitation. These outcomes may establish a new benchmark for noncircular journal bearings and demonstrate the role of nanoparticles in stabilizing hydrodynamic films under practical operating conditions with improved load-carrying capacity and cavitation control in industrial bearing systems.

Methodology

The three-lobe hydrodynamic journal bearing was first designed and modeled in SolidWorks CAD software using the geometrical and operating parameters. The final design dimensions, derived from a parametric study, were adopted for fabrication and the bearing was subsequently procured from Suntech Engineering Corporation, Kolkata (India). The bearing was then installed in a custom hydrodynamic journal bearing test setup to conduct experimental investigations under controlled operating conditions. These tests were performed to evaluate the hydrodynamic pressure distribution and load-carrying capacity during operation. The experimental data provided a baseline for validation of the numerical model.

In parallel, the simulations were carried out in ANSYS Fluent to predict the hydrodynamic pressure profile and cavitations with and without nanoparticle. The numerical predictions were systematically compared with experimental results to assess model accuracy and establish confidence in the CFD approach. Figure 1 illustrates the three-lobe bearing geometry, and all input parameters used in both experimental and numerical studies are summarized in Table 1. These include geometric dimensions, operating conditions, lubricant properties, and nanoparticle characteristics. Parameters were determined from direct experimental measurements, manufacturer specifications, and established literature sources. The eccentricity ratio presented in Table 1 was calculated from the applied design load of 1000 N using the Sommerfeld number derived from the bearing design analysis and interpolated from the Raimondi–Boyd charts for an L/D ratio of 1. The calculated eccentricity ratio of approximately 0.6 was used as the initial input for defining the oil film geometry in the CFD model. In the experimental study, tests were performed under a constant load of 1000 N and the inlet pressure was determined based on the design calculations. Thus, the eccentricity ratio served as a reference design parameter for numerical initialization, while the experimental investigation was governed by load and pressure control to maintain consistency between analytical, numerical, and experimental approaches.

In the CFD simulation, only the density and dynamic viscosity differed between the base oil and TiO_2 nanolubricant, as these parameters directly affect pressure generation

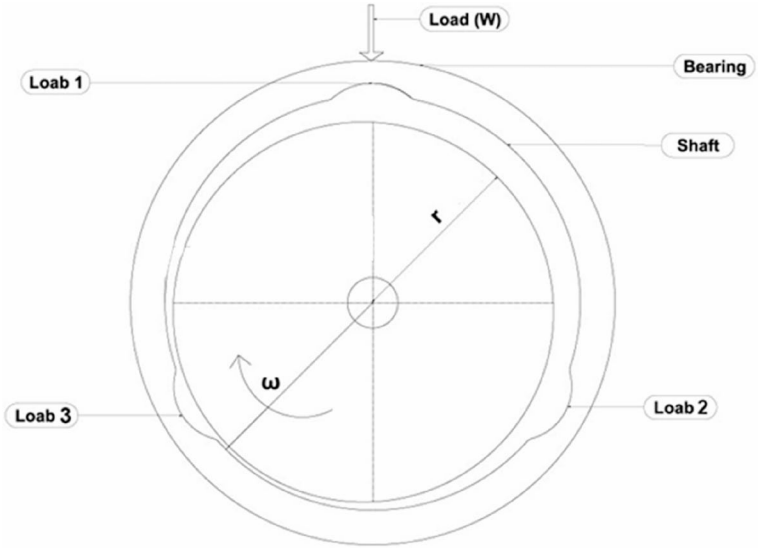

Fig. 1 The three-lobe bearing geometry

Table 1 Parameters used in the analysis

Category	Parameter	Symbol	Value
Geometry & Operating Conditions	Journal diameter	d	49.89 mm
	Bearing diameter	D	50 mm
	Radial clearance	C	0.055 mm
	Preload factor	δ	0.5
	Bearing length	L	50 mm
	L/D Ratio	-	1
	Rotational speed	N	500, 750, 1000 RPM
	Applied load	W	1000 N
	Inlet Pressure	P	0.4 MPa
	Eccentricity ratio	ε	0.6
Lubricant Properties	Lubricant	-	MOBIL DTE 24
	Lubricant viscosity	μ	0.0292 Pa·s
	Lubricant density	ρ	869 kg/m^3
	Vapor saturation pressure	P_v	0.018542 MPa
	Specific heat (lubricant)	C_p	1951 J/kg·K
Nanoparticle Properties (TiO_2 additive)	Nanoparticle type	-	TiO_2
	Concentration	-	0.5 wt.%
	TiO_2 nanoparticle size	-	40 nm (Range: 30–50 nm), Density (ρ) = 4230 kg/m^3
	Dynamic viscosity		0.0294 Pa·s
	Density of the TiO_2 nanolubricant		870 kg/m^3
Material Properties	Bearing material	-	C45 Steel: E = 200 GPa, ρ = 7870 kg/m^3, ν = 0.3
	Shaft material	-	EN8 Steel: E = 210 GPa, ρ = 7850 kg/m^3,

and film stability. Other properties, including specific heat and vapor pressure, were kept constant. The TiO_2 nanoparticle characteristics from Table 1 (density = 4230 kg/m^3, size = 40 nm) were incorporated through the effective property method, modeling the nanolubricant as a homogeneous fluid with modified effective properties at a 0.5 wt.% concentration.

Experimentation

The experimentation is carried out on a dedicated journal bearing test setup available at the research center (MET Institute of Engineering, Nashik, Maharashtra, India), specifically designed to support advanced hydrodynamic bearing studies. The setup provides a rigid and vibration-free platform that ensures precise control of operating parameters and accurate measurement of bearing characteristics. Owing to its modular design, the setup accommodates both circular and non-circular geometries, thereby enabling comparative performance evaluations under varied configurations. The set up consists of a precision journal assembly driven by a belt-coupled A.C. motor, an adjustable loading mechanism, and a closed-loop hydraulic lubrication unit illustrated in Fig. 2 (a). The lubricant, MOBIL DTE 24 oil, was delivered at a regulated inlet pressure of 0.4 MPa using a 0.5 hp gear pump, ensuring consistent film formation during testing. Pressure measurements were obtained using a Keller Series 35X transducer (full scale = 3 MPa; accuracy ± 0.1% FS → ± 0.003 MPa). Each test condition (speed and lubricant) was repeated three times, and the reported values represent the mean of three independent readings, while the plotted error bars denote ± 1 standard deviation (σ). These combined uncertainties accounting for both instrument precision and experimental repeatability lies in the range of ± 0.003–0.02 MPa, corresponding to approximately 0.3–3% of the

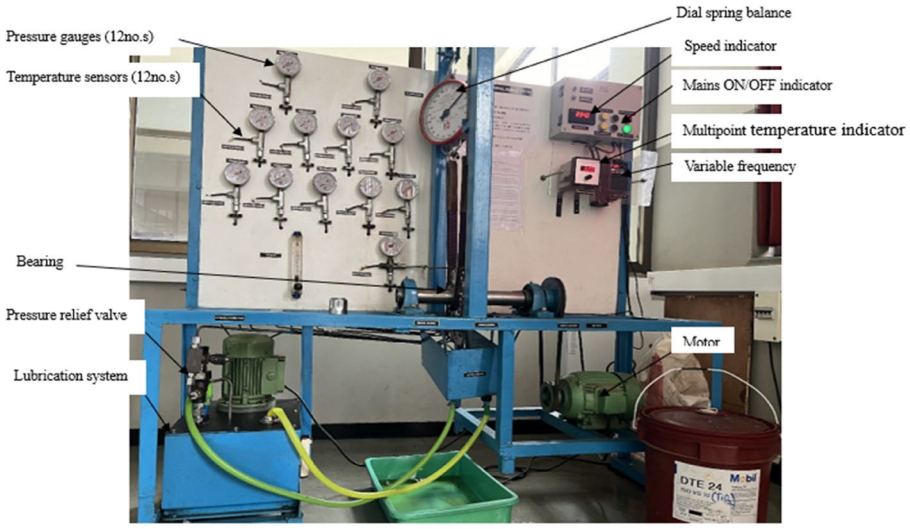

(a). Actual experimental test setup

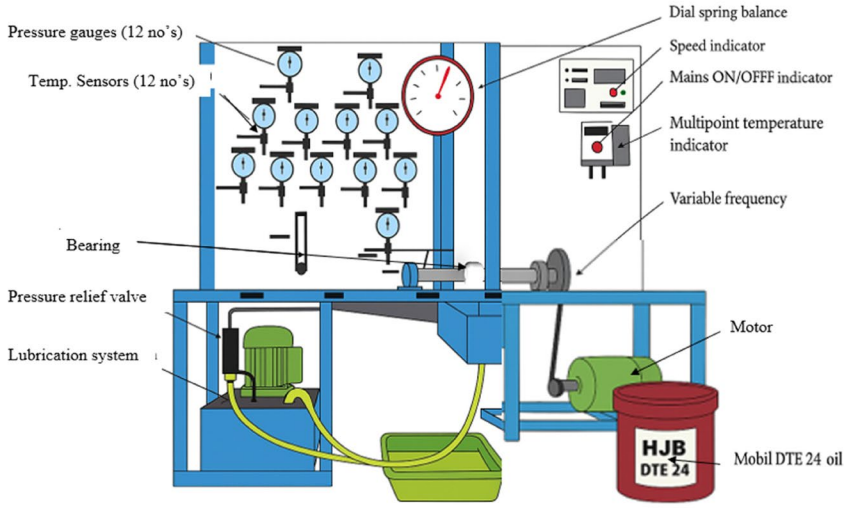

(b). A Schematic diagram of the test rig

Fig. 2 **a** Actual experimental test setup. **b** A Schematic diagram of the test rig

measured pressure, depending on angular position and load. To capture the circumferential pressure distribution, the bearing housing was fabricated with 12 pressure ports evenly spaced at 30° intervals. A schematic layout section of the test setup, including transducer positioning, shaft–bearing alignment, and data-acquisition arrangement, has been incorporated as shown in Fig. 2 (b) and the clear understanding of the pressure-sensor distribution along the bearing circumference as shown in Fig. 3.

TiO_2 nanolubricant (0.5 wt.%) was prepared by dispersing TiO_2 nanoparticles (30–50 nm, anatase phase; Nanolabs Ltd., India) in Mobil DTE 24 base oil. The mixture was mechanically stirred at 1500 rpm and magnetically agitated at 1200 rpm for 30 min to achieve uniform dispersion. Oleic acid was used as a surfactant to reduce surface energy and prevent nanoparticle agglomeration. The prepared nanolubricant remained visually stable without sedimentation for at least 4 h, covering all experimental runs. TiO_2

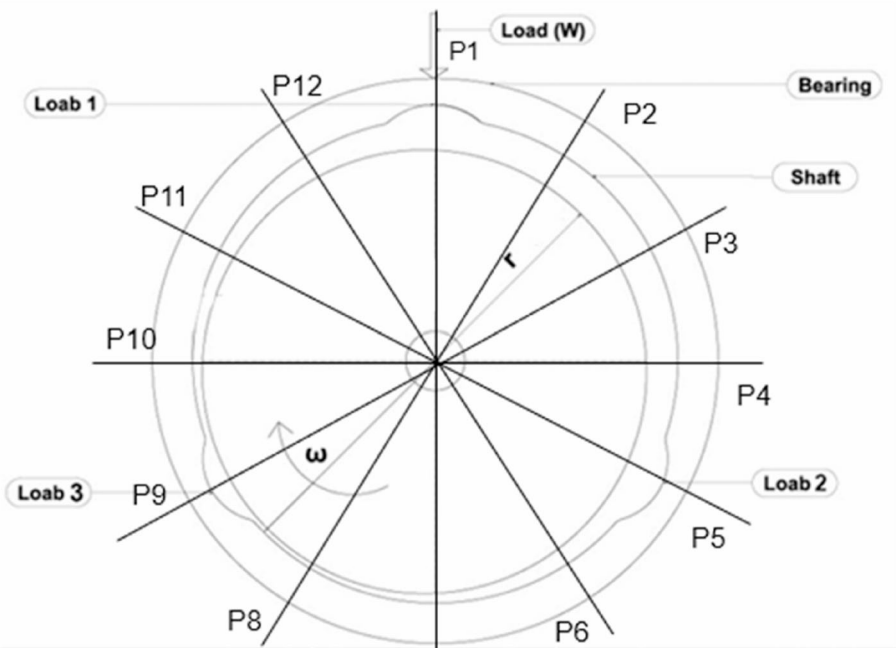

Fig. 3 Pressure sensors position

nanoparticles were selected due to their high thermal stability, low density, and inert interaction with the base oil and metallic surfaces [7, 9].

The addition of TiO_2 nanoparticles to the base lubricant primarily modifies its thermo-physical properties such as viscosity, density, and specific heat, without altering the overall fluid behavior or flow regime. The viscosity enhancement was experimentally verified and modeled using the modified Krieger–Dougherty correlation, consistent with the findings of Suryawanshi and Pattiwar [7], who confirmed Newtonian flow behavior even with TiO_2 additives up to 0.5 wt%. Hence, the mixture multiphase model and ZGB cavitation model remain valid for both base and nanolubricants, as they accurately capture pressure–vapor interactions in thin-film regions. The improved load capacity and reduced friction observed in CFD and experimental results are attributed to the higher viscosity and film strength rather than any fundamental change in flow characteristics.

Before experimentation, the system was initially operated for 30 min to attain mechanical and thermal stability, thereby minimizing transient effects and ensuring repeatable results. After steady-state conditions were established, the journal speed was adjusted using a variable frequency drive (VFD), and the load was applied through a calibrated spring balance. Pressure data were then recorded simultaneously from all twelve circumferential locations spanning 0° to 330°. The effect of temperature on lubricant viscosity was evaluated during the experimental trials, and it was found to be negligible under the selected test conditions. The bearing tests were performed at moderate speeds and medium load, where the oil film temperature rise measured near the bearing inlet and outlet was less than 5 °C. This small variation does not cause a significant change in the viscosity of Mobil DTE 24 or TiO_2 (0.5 wt.%) nanolubricant, confirming that isothermal conditions could be reasonably assumed for experimentation [7, 11, 12]. The measured pressure generated at each experimental conditions is presented in Table 2, while the corresponding plots of pressure generated are shown in Fig. 4.

Table 2 Experimental hydrodynamic pressures for base oil and 0.5% wt. TiO_2 nanolubricant

Angular position (°)	Mobil DTE24			0.5% wt. TiO_2 nanoparticles		
	Measured pressure (MPa)			Measured pressure (MPa)		
	500 RPM	750 RPM	1000 RPM	500 RPM	750 RPM	1000 RPM
0°/360° (Top)	0.40	0.40	0.40	0.40	0.40	0.40
30°	0.28	0.38	0.52	0.34	0.39	0.55
60°	0.33	0.45	0.58	0.48	0.49	0.61
90° (right)	0.36	0.52	0.67	0.58	0.63	0.73
120°	0.40	0.58	0.78	0.56	0.69	0.83
150°	0.41	0.59	0.78	0.58	0.73	0.87
180° (bottom)	0.42	0.64	0.88	0.66	0.79	1.06
210°	0.48	0.78	1.04	0.68	0.89	1.22
240°	0.22	0.11	0.13	0.38	0.50	0.93
270° (left)	−0.23	−0.32	−0.18	−0.18	0.16	0.66
300°	−0.42	−0.43	−0.28	−0.33	−0.08	0.47
330°	−0.39	−0.39	−0.20	−0.12	−0.09	0.28

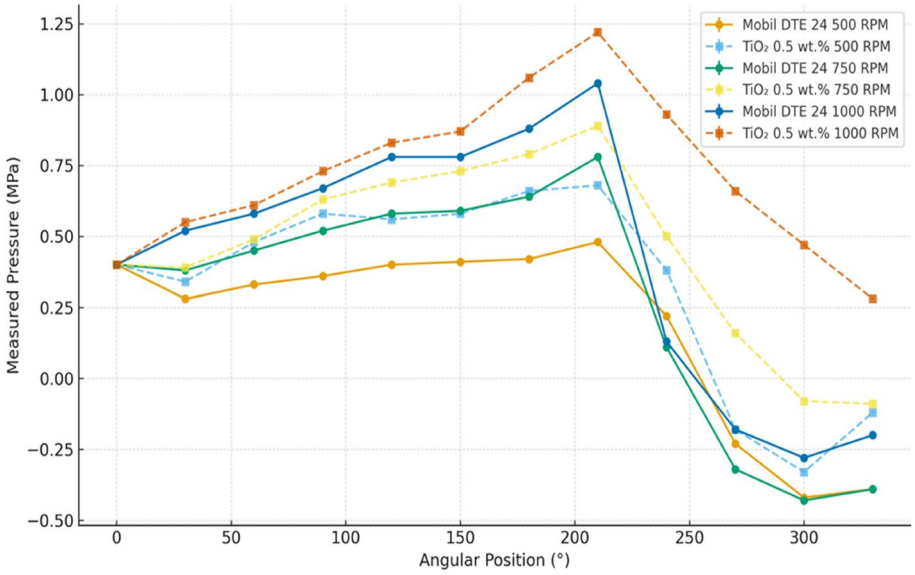

Fig. 4 Pressures generated at each experimental condition

The experimental findings revealed a pronounced influence of lubricant composition on the hydrodynamic performance of the three-lobe journal bearing. Compared to the base oil, the addition of 0.5 wt.% TiO_2 nanoparticles consistently elevated film pressures across all operating speeds (500, 750, and 1000 RPM). Notably, at 1000 RPM the peak pressure in the converging zone (210°) increased from 1.04 MPa with base oil to 1.22 MPa with the nanolubricant. This substantial pressure rise reflects the enhanced load-carrying capacity of the bearing and underscores the ability of the nanoparticles to suppress cavitation and stabilize the lubricant film under dynamic conditions. The improvements were more significant at higher rotational speeds, reflecting the stabilizing role of nanoparticles in sustaining the lubricant film.

CFD analysis

The CFD simulations were carried out to analyze pressure distribution, cavitation onset, and film behavior in the three-lobe journal bearing using both base oil (Mobil DTE 24) and TiO_2 nanolubricants. Figure 1 illustrates the three-lobe bearing geometry, and all input parameters used in numerical studies are summarized in Table 1. The simulation procedure followed a sequential workflow starting from geometry modeling and meshing to model selection, boundary condition setup, and solver initialization. Convergence was ensured through residual monitoring and pressure stabilization, followed by post-processing and validation with experimental data, as shown in Fig. 5.

Among multiphase approaches such as VOF, Eulerian, and DPM, the mixture model was selected for its balance of accuracy and computational efficiency in bearing applications. Unlike the traditional Reynolds equation approach, which assumes a single-phase incompressible flow and represents cavitation only through simplified pressure

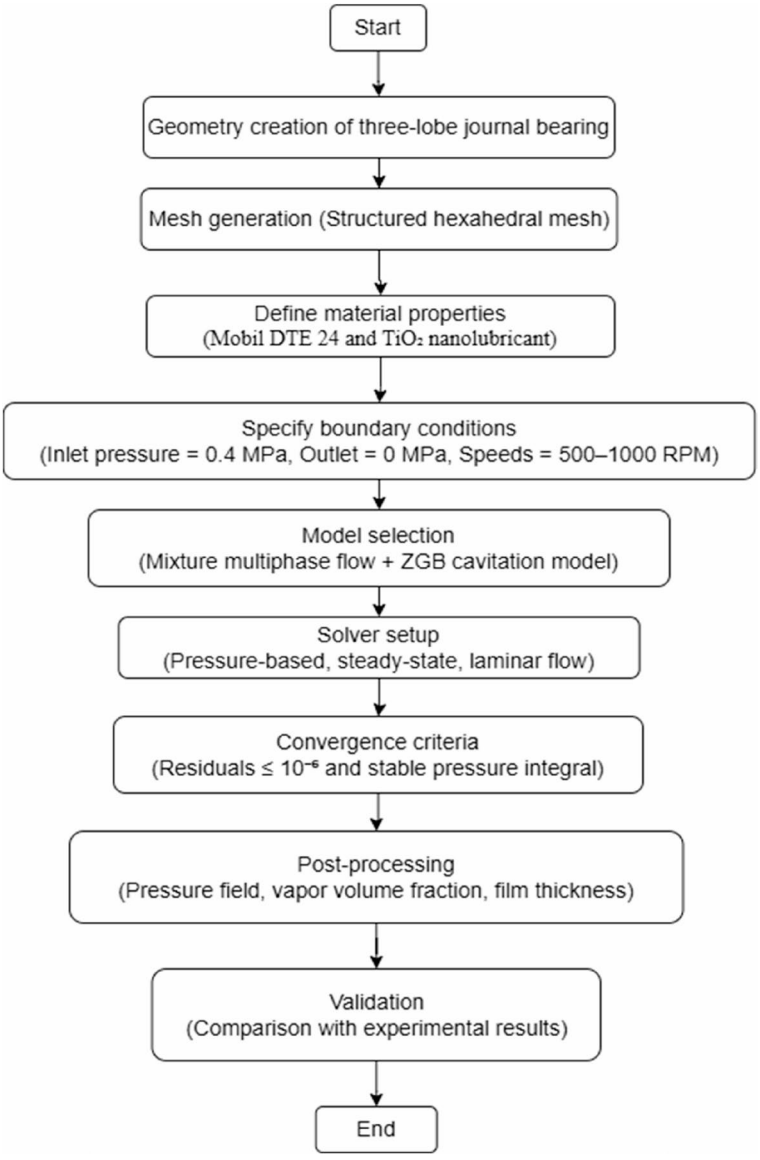

Fig. 5 Flow chart of numerical simulation process steps

boundaries [9, 14, 15], Cavitation was modeled using the Zwart–Gerber–Belamri (ZGB) formulation, which incorporates bubble nucleation, growth, and collapse dynamics with reported prediction errors below 5% [16]. The mixture–ZGB model simultaneously resolves liquid and vapor phases, allowing accurate prediction of vapor fraction and pressure recovery based on local pressure variation [11, 17]. This integrated model has also been validated for nanolubricant-based hydrodynamic bearings, confirming its reliability in capturing cavitation suppression and film stability effects [12].

The governing equations for bubble growth, vapor transport, and phase change mass transfer as given in Eqs. (1), (2), (3), (4), were derived from the Rayleigh–Plesset relation, with surface tension and bubble acceleration effects neglected, as these are insignificant for submicron bubbles typically present in hydrodynamic lubrication.

The resulting bubble growth rate is expressed as:

$$\frac{dR_b}{dt} = \sqrt{\frac{2}{3} \cdot \frac{p_b - p}{\rho_l}} \tag{1}$$

This relationship is embedded in the vapor transport equation:

$$\frac{\partial}{\partial t}\left(a_v \cdot \rho_v\right) + \nabla\left(a_v \cdot \rho_v \cdot v_v\right) = C_e - C_c \tag{2}$$

where, C_e and C_c account for the mass transfer between the liquid and vapor phases in cavitation, a_v is the vapor volume fraction, and is key to accurately representing local density variations in cavitated zones.

A microbubble radius of $R_b = 10^{-6}m$ was adopted, consistent with experimental pressure recovery observations at 300° and representative of entrapped microbubbles on machined C45 steel surfaces. The nucleation site volume fraction was set to $a_{nue} = 5 \times 10^{-4}$, based on the measured surface roughness of the test bearings. The evaporation and condensation coefficients were set to $F_{evap} = 50$ and $F_{cond} = 0.02$ to ensure stable convergence and accurate vapor generation rates [4, 18].

The model switches between evaporation $(P < P_v)$:

$$C_e = F_{evap} \cdot \frac{3 \cdot a_{nue}\left(1 - a_v\right) \cdot \rho_v}{R_b} \cdot \sqrt{\frac{2}{3}\frac{p_v - p}{\rho_l}} \tag{3}$$

and condensation modes $(P \geq P_v)$:

$$C_C = F_{cond} \cdot \frac{3 \cdot a_v \cdot \rho_v}{R_b} \cdot \sqrt{\frac{2}{3}\frac{p_v - p}{\rho_l}} \tag{4}$$

This configuration enabled accurate prediction of vapor formation in low-pressure zones and gradual collapse during re-pressurization. The hydrodynamic behavior of the three-lobe journal bearing was simulated in ANSYS Workbench 2024R1 by solving the fundamental conservation equations of mass and momentum (Eqs. 5, 6, 7). In order to realistically capture the fluid response inside the converging and diverging regions, lubricant viscosity was treated as a pressure–temperature dependent property rather than as a constant, following the model proposed [29]. This allowed the CFD model to account for the localized viscosity variations that directly influence pressure generation and cavitation formation within the thin film.

The lubricant film thickness was determined using Eq. (8), which integrates the effects of preload geometry, journal eccentricity and angular displacement of the shaft. Additionally, the formulation incorporates elastic deformation of the bearing surface, ensuring that compliance effects were reflected in the clearance distribution [4]. By combining these factors, the model was able to capture realistic film geometry under dynamic operating conditions. Flow regime characterization was carried out through calculation of the Reynolds number using Eq. (9). Across the tested speed range (500–1000 RPM), values were consistently below 2000, thereby confirming the laminar nature of the lubricant flow. This justified the exclusion of turbulence modeling, simplifying the computational effort without compromising accuracy. Finally, viscosity variation was further refined using the exponential pressure–temperature dependence given in Eq. (10).

Mass conservation:

$$\frac{\partial \rho}{\partial t} + \nabla \left(\rho \cdot \overrightarrow{v}\right) = 0 \tag{5}$$

where, ρ is fluid density and $\overrightarrow{v}$ is the fluid velocity vector.

Momentum conservation:

$$\frac{\partial(\rho \cdot \overrightarrow{v})}{\partial t} + \nabla \left(\rho \cdot \overrightarrow{v} \bullet \overrightarrow{v}\right) = -\nabla P + \nabla \left(\overline{\tau}\right) + \rho.\overline{g} + \overline{F} \tag{6}$$

where P is the static pressure, $\overline{\tau}$ is the stress tensor, $\rho.\overline{g}$ is the force due to gravity, and $\overline{F}$ is the external body force.

Stress tensor ($\overline{\tau}$):

$$\overline{\tau} = \mu[\left(\nabla \cdot \overrightarrow{v} + \nabla \cdot \overrightarrow{v}^{T}\right) - \frac{2}{3}\nabla \times \overrightarrow{v} \bullet I] \tag{7}$$

where, μ is the fluid viscosity and I is the unit tensor.

Equation (8) includes the elastic deformation term (δE) for completeness; however, in this study, the bearing and journal surfaces were assumed rigid, and δE was set to zero. This assumption is valid because the maximum pressure (≈1.5 MPa) induces negligible deformation in C45 steel (E = 200 GPa) compared to the minimum film thickness, and thus does not influence the hydrodynamic behavior.

Film thickness (h):

$$h = c_P - X \cdot cos\left(\theta\right) - Y \cdot sin\left(\theta\right) - \left(c_P - c_b\right) \bullet cos\left(\theta - \theta_P\right) + \delta_E \tag{8}$$

where, h is the film thickness, c_P is the preloaded radial clearance; X and Y are journal center displacements; θ is the angular position; c_b is the base circle clearance; θ_P is the preload (lobe) angle; and δ_E is elastic deformation.

Reynolds number (R_e):

$$R_e = \frac{\rho \cdot \omega \cdot R \cdot C_b}{\mu} \tag{9}$$

Values between 4.28 and 8.56 across the tested speeds confirm laminar flow, well below the turbulent threshold ($R_e < 2000$).

Viscosity model:

$$\mu = \mu_0 e^{\alpha(P-P_0)} e^{\beta(T-T_0)} \tag{10}$$

where α and β are empirical pressure and temperature coefficients.

The SIMPLEC algorithm was used for pressure–velocity coupling, while second-order upwind discretization ensured accuracy in momentum and volume fraction equations. Convergence was considered achieved when continuity and momentum residuals dropped below 1×10^{-6} and integral pressure values stabilized. This framework enabled reliable prediction of hydrodynamic pressure buildup and cavitation suppression. Boundary conditions applied for CFD analysis are same as that of experimental conditions; a summary of the simulation setup and boundary conditions is provided in Table 3. Since, experimental observations revealed marginal rise in lubricant temperature during the working conditions at varying speed. The CFD simulations were conducted under isothermal assumptions, since the viscosity variations within this limited temperature range (< 5 °C) had an insignificant influence on hydrodynamic pressure and film stability. Similar simplifications have been adopted in prior studies on noncircular and multi-lobe bearings operating under comparable conditions, where thermal coupling showed minimal impact on the pressure field [9, 14, 15, 17]. This approach also reduces computational complexity without compromising accuracy.

Mesh configuration

The computational domain was discretized using a structured hexahedral mesh consisting of 415,716 control volumes. The structured grid was designed to conform closely to the bearing geometry, minimizing interpolation errors and accurately resolving steep pressure and velocity gradients within the thin lubrication film. To capture viscous effects near the wall, seven inflation layers were introduced with a first-layer thickness of 1 μm, maintaining the non-dimensional wall distance ($y^* < 1$) within the viscous sublayer. Although the flow is laminar, such near-wall refinement is crucial for accurate prediction of shear stresses and pressure buildup in the film region. This meshing strategy is consistent with lubrication flow analyses reported by [9, 14, 17]. This configuration allowed the model to capture pressure build-up and shear stresses within the film with high fidelity. In the load-controlled CFD simulations, a dynamic mesh update strategy was applied to

Table 3 CFD simulation setup and boundary conditions

Parameter	Specification
Software	ANSYS Workbench 2024R1
Solver type	Pressure-based, 3D, double precision, steady-state
Flow regime	Laminar
Cavitation model	Zwart–Gerber–Belamri (ZGB)
Multiphase model	Mixture model with vapor transport
Inlet boundary	Pressure inlet, gauge pressure = 0.4 MPa at 0°
Outlet boundary	Pressure outlet, atmospheric pressure
Journal wall	Rotating wall (500, 750, 1000 RPM), no-slip condition
Bearing wall	Stationary, no-slip condition
Mesh configuration	Structured hexahedral, 415,716 cells
Near-wall resolution	7 layers; first-layer thickness = 1 μm
Mesh quality	Skewness: 0.16–0.85 (maintained < 0.3 in critical hydrodynamic regions)
Pressure–velocity coupling	SIMPLEC algorithm
Spatial discretization	Second-order upwind (momentum, volume fraction)
Convergence criteria	Residuals ≤ 1×10^{-6} (continuity, momentum) with stabilization of integral pressures

maintain force equilibrium between the applied load and the hydrodynamic reaction. The structured hexahedral mesh shown in Fig. 6 was generated with local refinement in the lubrication film region. During simulation, the journal position was iteratively adjusted, and the mesh was automatically deformed using a spring-based smoothing and local remeshing algorithm in ANSYS Fluent to preserve element quality and orthogonality. This process continued until the resultant hydrodynamic force matched the 1000 N load within 0.1% residual error. The adopted approach ensured accurate prediction of the equilibrium eccentricity and film profile without mesh distortion or numerical instability.

Mesh quality was assessed using skewness, which was varied between 0.16 and 0.85 across the computational domain. In the critical hydrodynamic regions particularly the converging zone where peak pressures are generated and the diverging zone susceptible to cavitation skewness values remained below 0.3, thereby minimizing numerical diffusion and promoting stable convergence of the governing equations. A mesh independence study was carried out to confirm grid adequacy and successive mesh refinements were tested, and the observed variations in peak pressure and vapor volume fraction were less than 2%. This established that the adopted mesh offered an optimal balance between computational efficiency and solution accuracy, ensuring reliable results across all simulated operating speeds.

Pressure and cavitation in journal bearings

Figure 7 (a-c) presents pressure contours obtained from the simulations, where consistent trend was observed across all operating speeds. The addition of TiO_2 nanoparticles enhanced peak pressures in the converging regions while simultaneously mitigating negative pressures in the diverging zones. Figure 7(a) shows the addition of

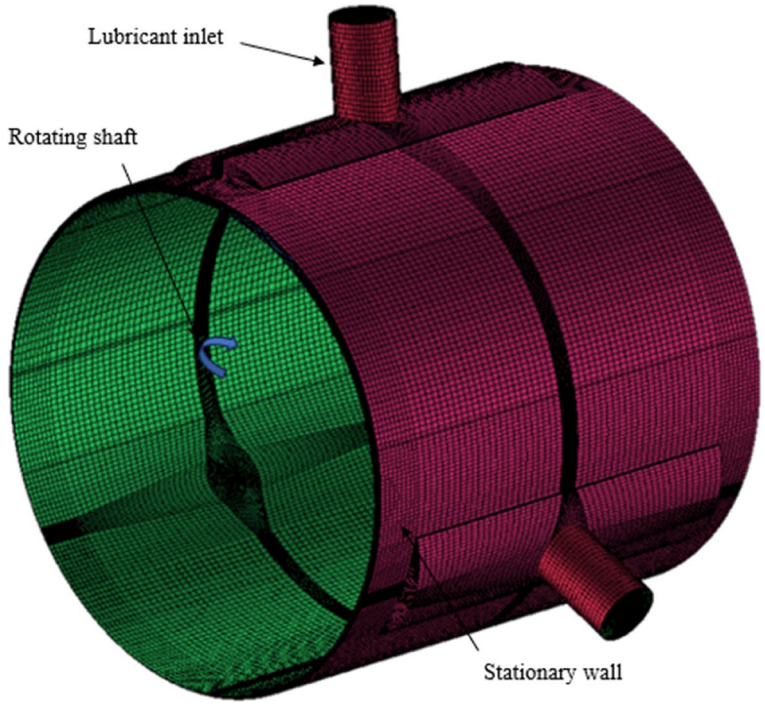

Fig. 6 The structured hexahedral mesh

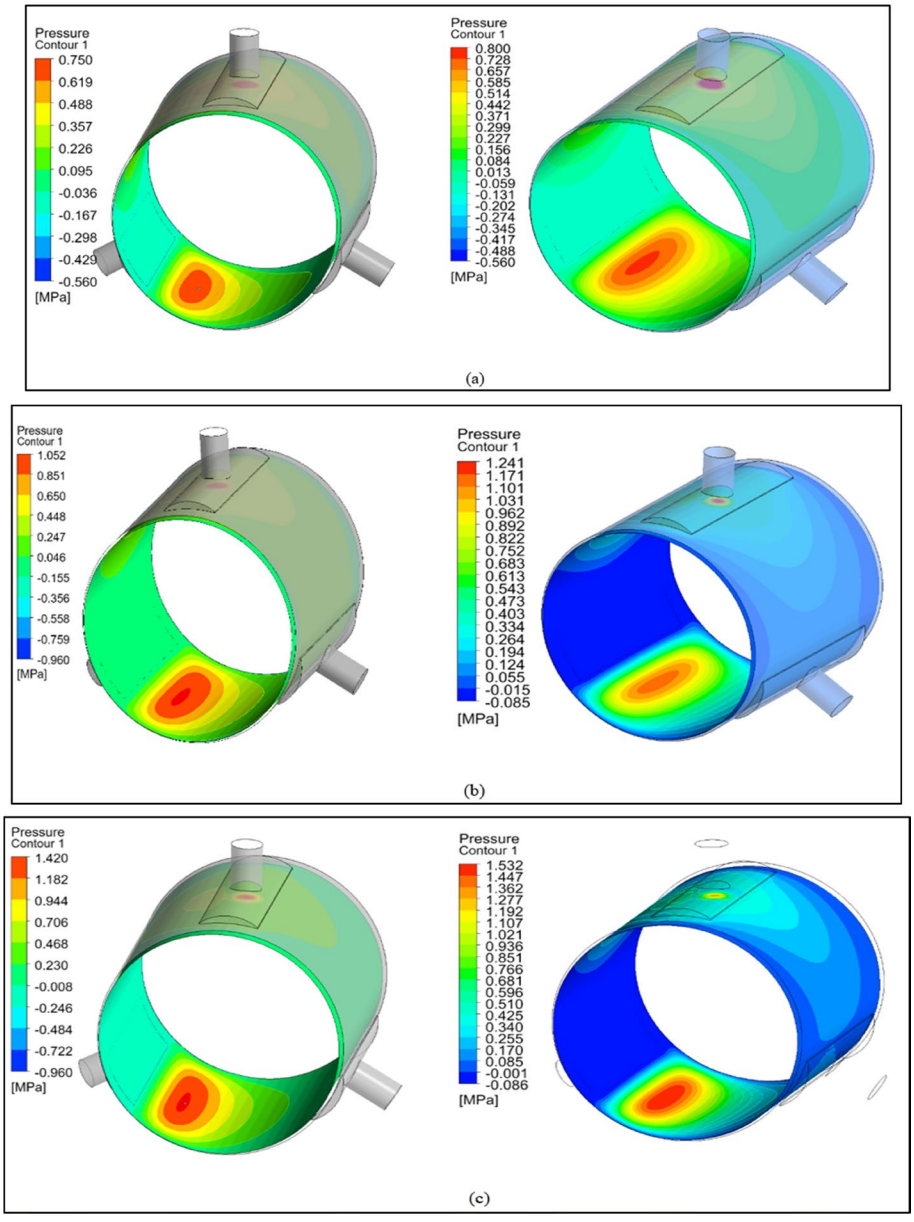

Fig. 7 CFD predicted pressure contours at (**a**) 500 RPM, (**b**) 750 RPM, and (**c**) 1000 RPM, comparing base oil(left) and TiO_2 nanolubricant(right)

TiO_2 nanoparticles increased peak pressures in the converging zones and reduced the extent of vapor cavities, indicating early cavitation suppression compared to base oil at 500 RPM.

Figure 7(b) shows the nanolubricant further elevated hydrodynamic pressures while significantly diminishing negative-pressure regions, showing a stronger stabilizing effect on the lubricant film at 750 RPM. Figure 7(c) shows cavitation pockets were nearly eliminated with the nanolubricant, demonstrating its ability to sustain film stability and pressure under higher dynamic loads at 1000 RPM.

For comparison, pressure values were extracted from the CFD simulations at 12 circumferential locations (0°–330° at 30° intervals), corresponding to the pressure transducer positions in the experimental setup which is summarized in Table 4.

Table 4 CFD-predicted pressure distribution for base oil and TiO_2 nanolubricant

Angular position (°)	Mobil DTE24			0.5% wt. TiO_2 nanoparticles		
	Observed pressure (MPa) at various speed			Observed pressure (MPa) at various speed		
	500 RPM	750 RPM	1000 RPM	500 RPM	750 RPM	1000 RPM
0°/360° (Top)	0.4	0.4	0.4	0.4	0.4	0.4
30°	0.3	0.41	0.55	0.36	0.42	0.58
60°	0.35	0.48	0.62	0.51	0.53	0.65
90° (Right)	0.38	0.56	0.72	0.62	0.68	0.78
120°	0.42	0.61	0.82	0.59	0.73	0.88
150°	0.43	0.63	0.84	0.61	0.78	0.92
180° (Bottom)	0.44	0.68	0.94	0.70	0.84	1.12
210°	0.5	0.82	1.1	0.72	0.95	1.3
240°	0.23	0.12	0.14	0.4	0.54	1
270° (Left)	–0.25	–0.35	–0.20	–0.20	0.17	0.7
300°	–0.45	–0.46	–0.30	–0.35	–0.09	0.5
330°	–0.42	–0.42	–0.22	–0.13	–0.10	0.3

Results and discussion

The combined experimental and numerical analyses revealed that dispersing 0.5 wt.% TiO_2 nanoparticles into Mobil DTE 24 oil markedly enhanced the hydrodynamic performance of the three-lobe journal bearing. The improvement stems from the rheological modification, interfacial enhancement, and thermal effects introduced by TiO_2 nanoparticles, which alter the lubricant's viscosity, surface tension, and heat-transfer behavior. The nanoparticles increased the effective viscosity and film stiffness, thereby stabilizing the pressure field and preventing local pressure drops below vapor pressure. Their spherical anatase morphology improved surface wettability and reduced interfacial tension, suppressing vapor nucleation and bubble growth. Furthermore, the enhanced thermal conductivity of the nanolubricant facilitated localized heat dissipation, limiting vapor formation in low-pressure regions. These synergistic effects collectively extended the full-film lubrication regime, reduced vapor fraction intensity, and improved load-carrying stability. Similar cavitation suppression mechanisms for oxide-based nanolubricants have been reported by Awad et al. [7], Abass et al. [9], Biswas et al. [14], and Tauviqirrahman et al. [17].

A detailed comparison of pressure distributions at twelve circumferential locations (0°–330°, at 30° intervals) presented in Fig. 8 (a–c) confirmed excellent correlation between experimental and CFD results. At 500 RPM, the CFD model accurately captured pressure peaks and cavitation onset; at 750 RPM, both datasets exhibited a nonlinear pressure rise with clear suppression of negative pressures; and at 1000 RPM, the agreement remained strong, with deviations within ± 6% across all conditions. This consistency validates the reliability of the developed CFD framework in predicting nanoparticle-induced hydrodynamic improvements.

The experimental and CFD results consistently showed higher film pressures and improved cavitation resistance with the TiO_2 nanolubricant across all operating speeds (500–1000 RPM). Compared with the base oil, the nanolubricant significantly increased peak pressures in the converging zones while alleviating negative pressures in the diverging regions. At 1000 RPM, the maximum pressure at the 210° location rose from 1.04 MPa (base oil) to 1.22 MPa (nanolubricant) in experiments, and from 1.10 MPa to 1.30 MPa in CFD simulations, while the minimum pressure approached zero confirming

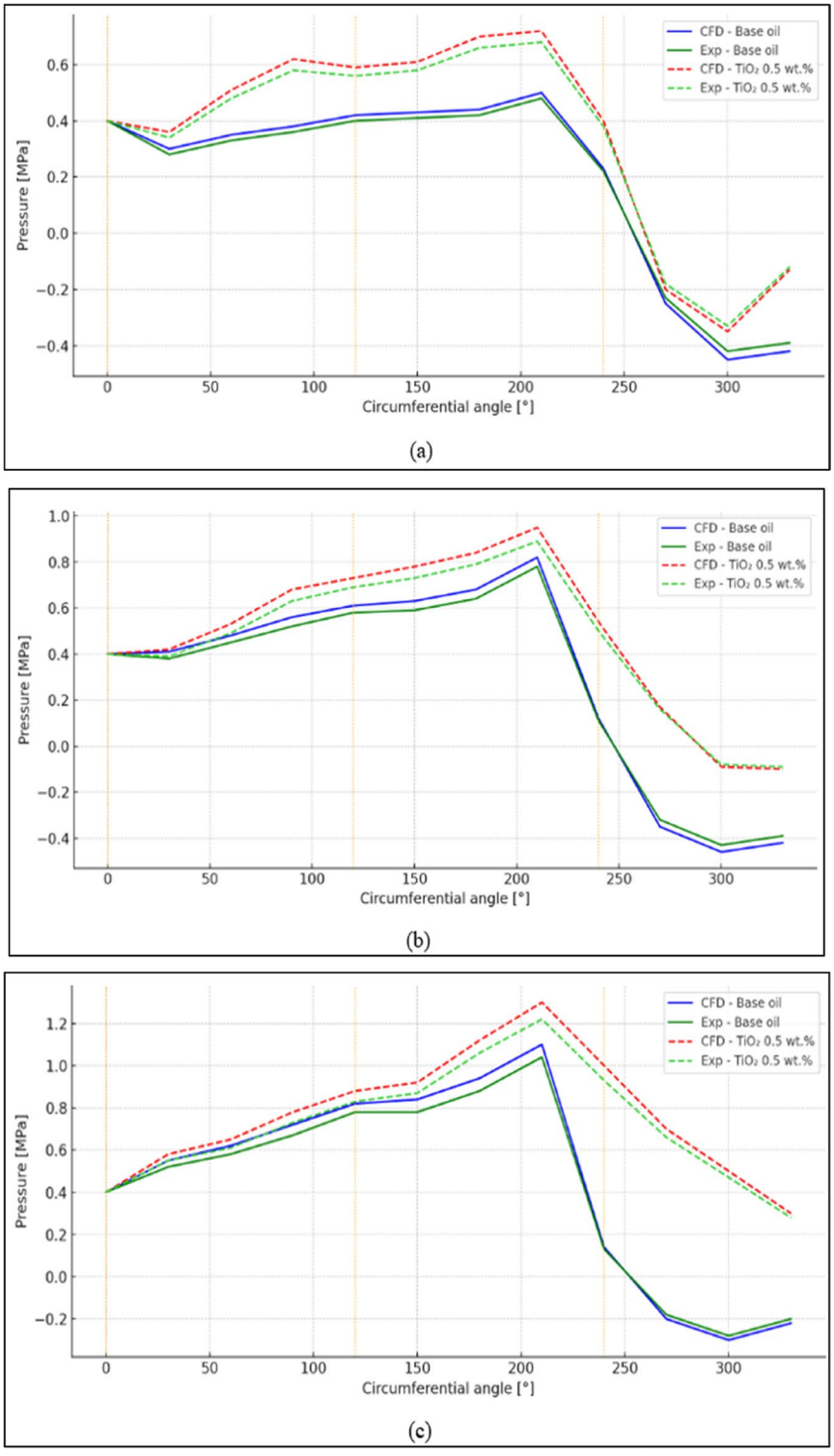

Fig. 8 Comparison of experimental and CFD pressure distributions at (**a**) 500RPM, (**b**) 750RPM and (**c**) 1000RPM

effective cavitation suppression and improved film continuity. A localized high-pressure region (~1 MPa) was also observed near the inlet due to hydrodynamic wedge formation from journal rotation within the converging film. This amplification, exceeding the supply pressure (0.4 MPa), is characteristic of noncircular bearings and aligns with

earlier findings by Abass et al. [9] and Tauviqirrahman et al. [17]. The improvement was more pronounced at higher speeds, reflecting the nanoparticles' stabilizing role under elevated shear and thermal conditions. The CFD pressure contours further revealed that vapor cavities diminished with increasing speed and were nearly eliminated at 1000 RPM, demonstrating the enhanced film integrity achieved with the nanolubricant. These enhancements directly translated into greater load-carrying capacity and reduced risk of film rupture.

Overall, the CFD framework effectively captured the coupled liquid–vapor interactions within the bearing clearance. The strong experimental–numerical agreement confirmed the suitability of the mixture multiphase model coupled with the Zwart–Gerber–Belamri (ZGB) cavitation formulation for noncircular geometries. The TiO_2 nanolubricant enhanced hydrodynamic pressure distribution, suppressed vapor fraction formation, and ensured smoother film continuity, confirming its effectiveness in improving load stability and cavitation resistance in multi-lobe bearings. The validated CFD model further provided physical insight into the underlying cavitation dynamics. It accurately predicted the onset, growth, and collapse of vapor cavities, and reproduced the nonlinear variation of pressure with rotational speed. The reliability of the ZGB model for cavitating flow in noncircular bearings is well supported by previous investigations [6, 10, 14]. Comparative analysis with earlier studies (Table 5) highlights that the present three-lobe bearing lubricated with 0.5 wt.% TiO_2 nanofluid (L/D = 1.0) achieved approximately 15–18% higher peak pressure and substantially improved cavitation resistance relative to prior oxide-based nanolubricants.

Conclusions

1. The addition of 0.5 wt.% TiO_2 nanoparticles to Mobil DTE 24 oil improved hydrodynamic performance by increasing peak pressures, suppressing cavitation, and enhancing load-carrying stability across 500–1000 RPM.
2. CFD simulations using the mixture multiphase model with the ZGB cavitation approach showed close agreement with experiments (within ± 6%), confirming the reliability of the numerical framework.
3. Circumferential pressure analysis revealed that TiO_2 nanoparticles were most effective in diverging regions, where they reduced negative pressures, stabilized the lubricant film, and minimized cavitation occurrence.
4. The use of TiO_2 nanolubricant promoted uniform pressure distribution and sustained film thickness at higher speeds, contributing to improved bearing performance.
5. The integrated experimental and CFD approach established a benchmark for three-lobe bearings with nanolubricants, offering predictive capability, reducing extensive testing needs, and guiding design optimization for improved bearing life and stability.
6. From an industrial viewpoint, the results demonstrate the potential of TiO_2 nanolubricants to enhance the efficiency and reliability of high-speed rotating equipment such as turbines, compressors, and precision spindles by mitigating cavitation and improving film stability.
7. Future direction should focus on incorporating thermo-hydrodynamic coupling, transient analysis, optimization of nanoparticle concentration and geometry, comparative evaluation with other nanolubricants.

Table 5 Comparison of key findings with earlier studies

Reference	Lubricant/Nanoparticles	Bearing Type	Method/Model	Key Findings	Improvement
[7]	TiO_2/SAE 40	Elliptical	Experimental	TiO_2 nanolubricant improved load capacity and reduced wear scar diameter by 10%	Focused on wear and friction; no CFD or cavitation modeling
[9]	CuO/SAE 40	Cylindrical	CFD (Reynolds equation)	CuO nanoparticles increased load capacity by 8%	No experimental validation; limited cavitation prediction
[14]	Al_2O_3/ISO VG 46	Two-lobe	CFD + Experimental	Al_2O_3 nanolubricant improved pressure stability and reduced temperature rise by 5 °C	Did not model vapor fraction or cavitation zones
[17]	ZnO/VG 68	Multi-lobe	CFD (ZGB cavitation model)	ZnO nanoparticles increased pressure by 10% and delayed cavitation onset	No experimental confirmation provided
[13]	TiO_2/SAE 30	Cylindrical	Experimental	TiO_2 reduced wear scar diameter by 12% and enhanced film strength	No CFD validation or pressure field analysis
Present Study	TiO_2 (0.5 wt.%)/Mobil DTE 24	Three-lobe (non-circular)	Experimental + CFD (ZGB)	TiO_2 nanolubricant increased peak pressure by 15–18%, suppressed cavitation, and enhanced load stability	First combined experimental–CFD validation for TiO_2 nanolubricant in a three-lobe bearing (L/D = 1.0)

Nomenclature

ρ Fluid density
$\overrightarrow{v}$ Fluid velocity vector
P Static pressure
τ Stress tensor
μ Dynamic viscosity
I Unit tensor
h Film thickness
c_P Preloaded radial clearance
c_b Base circle clearance
θ Angular position
θ_P Preload (lobe) angle
δ_E Elastic deformation
R_e Reynolds number
C_c Condensation rate
F_{evap} Evaporation coefficient
F_{cond} Condensation coefficient
a_{nue} Nucleation site volume fraction
β Temperature-viscosity coefficient
R_b Bubble radius
a_v Vapor volume fraction
C_e Evaporation rate
ω Angular velocity
R Bearing radius
μ_0 Reference viscosity
α Pressure-viscosity coefficient

Acknowledgements
The authors gratefully acknowledge the Research Center, Department of Mechanical Engineering, MET's Institute of Engineering, Nashik, for providing the laboratory facilities, technical support, and experimental setup essential to this investigation. Special thanks are also extended to Suntech Engineering Corporation, Kolkata (India), for sponsoring the three-lobe journal bearing, which was fabricated from C45 medium-carbon steel and designed with 12 equidistant threaded ports to accommodate sensor mounting along the bearing circumference.

Authors' contributions
First Author: Conceptualization, methodology, experimentation, CFD modeling, data analysis, and manuscript drafting.
Second Author: Conceptualization, supervision, guidance, and manuscript review and editing.

Funding
This study did not receive any specific grant from funding agencies in the public, commercial, or not-for-profit sectors.

Data availability
The datasets generated during the current study are available from the corresponding author upon reasonable request.

Declarations

Competing interests
The authors declare no known financial or personal conflicts of interest that could have influenced this work.

Received: 3 September 2025 / Accepted: 16 November 2025
Published online: 09 January 2026

References

1. Roy L, Kakoty SK (2015) Application of genetic algorithm in optimization of hydrodynamic bearings. In: Bansal S, Mandal J, Das S, Nagar A, Deep K (eds) Proceedings of Fourth International Conference on Soft Computing for Problem Solving: SocProS 2014, Volume 1, pp 207–217. Springer India. https://doi.org/10.1007/978-81-322-2220-0_18

2. Biswas N, Chakraborti P, Belkar S (2016) An analytical and experimental approach for pressure distribution analysis of a particular lobe and plain bearing performance keeping in view of all impeding varying parameters associating with fixed lubrication SAE20W40. J Mech Sci Technol 30:2187–2193. https://doi.org/10.1007/s12206-016-0435-4
3. El-Saida B, El-Souhily W, Crosby W, El-Gamal H (2017) The performance and stability of three-lobe journal bearing textured with micro protrusions. Alex Eng J 56(4):423–432. https://doi.org/10.1016/j.aej.2017.08.003
4. Dhande Y, Pande DW, Lanjewar GH (2018) Numerical analysis of three-lobe hydrodynamic journal bearing using CFD–FSI technique based on response surface evaluation. J Braz Soc Mech Sci Eng. https://doi.org/10.1007/s40430-018-1311-5
5. Chetti B, Crosby WA (2019) Preload effects on the static characteristics of three-lobe journal bearings lubricated with a couple stress fluid. Ind Lubr Tribol 71(10):1136–1143
6. Narwat K, Kumar V, Singh SJ, Kumar A (2025) Dynamic analysis of textured surface three-lobe hydrodynamic journal bearing operating with electro-rheological lubricant. Proceedings of the Institution of Mechanical Engineers, Part J: Journal of Engineering Tribology. https://doi.org/10.1177/13506501251330028
7. Suryawanshi SR, Pattiwar JT (2019) Experimental study on an influence of bearing geometry and TiO_2 nanoparticle additives on the performance characteristics of fluid film lubricated journal bearing. Tribol Ind 41(2):250–259
8. Dhanola R, Garg HC (2021) Experimental analysis of the efficacy of vegetable oil-based nanolubricants for improving journal-bearing performance. Proc Inst Mech Eng Part J J Eng Tribol 235(9):1974–1991. https://doi.org/10.1177/1350650120981478
9. Abass BA, Ahmed SY, Yaser MA (2023) Performance analysis of elliptical journal bearing lubricated with experimentally characterized nano-lubricant considering thermal effect using CFD technique. FME Trans 51(4):550–563.
10. Gundarneeya TP, Vakharia DP (2021) Performance analysis of journal bearing operating on nanolubricants with TiO_2, CuO and Al_2O_3 nanoparticles as lubricant additives. Mater Today Proc 45:5624–5630
11. Biswas N, Mandal SK, Bhagwatkar I, Kumar R, Kaur J, Bhowmik A, Bhattacharjee B (2025) Effect of nanoparticle-based lubricants on various performance characteristics of journal bearings: a review. Eng Res Express. https://doi.org/10.1088/2631-8695/ada8f7
12. Awad H, Abdou KM, Saber E (2025) The effect of axial geometrical variations on the steady state characteristics of oil lubricated journal bearings using TiO_2 nanoparticles as lubricant additives. Sci Rep 15(1):15701
13. Shaltout ML, Hegazi HA (2021) Multi-objective design optimization of HJBs using a hybrid approach. Ind Lubr Tribol 73(7):1052–1060. https://doi.org/10.1108/ILT-05-2021-0194
14. Dhande DY, Pande DW (2016) Multiphase flow analysis of hydrodynamic journal bearing using CFD coupled fluid structure interaction considering cavitation. J King Saud Univ-Eng Sci 30(4):345–354. https://doi.org/10.1016/j.jksues.2016.04.005
15. Chen Y, Sun Y, He Q, Feng J (2019) Elastohydrodynamic behavior analysis of journal bearing using fluid–structure interaction considering cavitation. Arab J Sci Eng 44:1305–1320. https://doi.org/10.1007/s13369-018-3442-3
16. Rasep Z, Yazid MNAWM, Samion S (2021) A study of cavitation effect in a journal bearing using CFD: a case study of engine oil, palm oil and water. J Tribol 28:48–62
17. Tauviqirrahman M, Wijaya M, Muchammad M, Paryanto P, Jamari J (2024) Hydrodynamic lubrication analysis of journal bearing considering cavitation, slip and thermal condition. J Tribol 42:1–20
18. Dong J, Wen H, Zhu J, Guo J, Zong C (2024) Analysis of thermo-hydrodynamic lubrication of three-lobe semi-floating ring bearing considering temperature–viscosity effect and static pressure flow. Lubricants 12(4):140. https://doi.org/10.3390/lubricants12040140
19. Wu YY, Tsui WC, Liu TC (2007) Experimental analysis of tribological properties of lubricating oils with nanoparticle additives. Wear 262(7–8):819–825. https://doi.org/10.1016/j.wear.2006.08.021
20. Dang RK, Chauhan A, Dhami SS (2021) Static thermal performance evaluation of elliptical journal bearings with nanolubricants. Proc Inst Mech Eng Part J J Eng Tribol 235(8):1627–1640
21. Abass BA, Ahmed SY, Kadhim ZH (2023) Analysis and optimization of nanolubricated journal bearing under thermoelastohydrodynamic lubrication considering cavitation effect. Tribol Ind 45(4):618
22. Lotfizadeh Dehkordi A, Ghadimi A, Metselaar HSC (2013) Box–Behnken experimental design for investigation of stability and thermal conductivity of TiO_2 nanofluids. J Nanopart Res 15(1). https://doi.org/10.1007/s11051-012-1369-4
23. Galda L, Sep J, Olszewski A, Zochowski T (2019) Experimental investigation into surface texture effect on journal bearings performance. Tribol Int 136:372–384. https://doi.org/10.1016/j.triboint.2019.03.073
24. Silva FV, Zanardi MA, de Souza TM (2021) Analytical–numerical modeling of journal bearings with non-Newtonian fluids and cavitation effects. J Braz Soc Mech Sci Eng. https://doi.org/10.1007/s40430-021-03238-4
25. Kouider M, Djallel Z, Abdelkader Y, Sahraoui K (2021) Mathematical modeling of journal bearing lubricated with non-Newtonian fluid. Tribol Ind 43(4):615–627
26. Mishra S, Aggarwal S (2023) A critical review of the effect of nano-lubricant on the performance of hydrodynamic journal bearing. Tribologia–Finn J Tribol 40(4). https://doi.org/10.30678/fjt.127785
27. Jose J, Behera N (2018) A review on non-circular journal bearings. Int J Mech Prod Eng Res Dev (IJMPERD) 8(1):207–220. https://doi.org/10.24247/ijmperdfeb201825
28. Kumar A, Kakoty SK (2019) A variable viscosity technique for the analysis of static and dynamic performance parameters of three-lobe fluid film bearing operating with TiO_2-based nanolubricant. In: Manufacturing Engineering: Select Proceedings of CPIE 2018, pp 1–16. Springer Singapore
29. Singla A, Kumar A, Bala S, Singh P, Chauhan A (2014) Thermo-hydrodynamic analysis on temperature profile of circular journal bearing using computational fluid dynamics. In: 2014 Recent Advances in Engineering and Computational Sciences (RAECS), pp 1–6. IEEE. https://doi.org/10.1109/RAECS.2014.6799526

Publisher's Note